Tuneable presynaptic weighting in optoelectronic spiking neurons built with laser-coupled resonant tunneling diodes

Weikang Zhang[1], Matěj Hejda[1], Ekaterina Malysheva[2], Qusay Raghib Ali Al-Taai[3], Julien Javaloyes[4], Edward Wasige[3], José M. L. Figueiredo[5], Victor Dolores-Calzadilla[2], Bruno Romeira[6], Antonio Hurtado[1]

[1] Institute of Photonics, SUPA Dept of Physics, University of Strathclyde, Glasgow, U.K.
[2] Eindhoven Hendrik Casimir Institute, Eindhoven University of Technology, Eindhoven, The Netherlands
[3] High Frequency Electronics Group, University of Glasgow, Glasgow, United Kingdom
[4] Dept de Física and IAC-3, Universitat de les Illes Balears, Palma de Mallorca, Spain
[5] Centra-Ciências and Departamento de Física, Faculdade de Ciências, Universidade de Lisboa, Lisboa, Portugal
[6] INL – International Iberian Nanotechnology Laboratory, Ultrafast Bio- and Nanophotonics Group, Braga, Portugal

E-mail: `submissions@iop.org`

Abstract. Optoelectronic artificial spiking neurons are regarded as promising core elements for novel photonic neuromorphic computing hardware. In this work, we investigate a modular optoelectronic spiking neuron built with an excitable resonant tunneling diode (RTD) coupled to a photodetector and a vertical-cavity surface-emitting laser (VCSEL). This work provides the first experimental demonstration of amplitude control of the fired optical spikes in the electrical-to-optical (E-O) part of the artificial neuron, therefore introducing a simple way of weighting for the presynaptic spikes. This is achieved by tuning the VCSEL bias current, hence providing a straightforward, high-speed, hardware-friendly option for the weighting of optical spiking signals. Furthermore, we validate the feasibility of this layout using a simulation of a monolithically integrated, RTD-based nanoscale optoelectronic spiking neuron model, which confirms the system's capability to deliver weighted optical spiking signals at GHz firing rates. These results demonstrate a high degree of flexibility of RTD-based artificial optoelectronic spiking neurons and highlight their potential towards compact, high-speed photonic spiking neural networks and light-enabled neuromorphic hardware.

Keywords: neuromorphic photonics, optoelectronic spiking neurons, photonic synapses, vertical-cavity surface emission laser, VCSEL, resonant tunneling diode, RTD.

1. Introduction

In recent decades, research in artificial intelligence (AI) has experienced significant advances driven by the rapid expansion of amounts of available data and cheaper, readily available computational power. The field of neuromorphic (brain-like) engineering, which incorporates a range of disciplines and aims at mimicking the operating mechanism of biological brains to achieve more efficient computing and AI systems, is undergoing intensive research effort. In particular, photonics-based neuromorphic platforms promise high bandwidth and operation speeds, along with lower attenuation losses, negligible crosstalk effects, and heating issues [1]. In the meantime, well-established semiconductor fabrication and optical communication technologies as well as a variety of miniaturized optical/optoelectronic devices provide considerable flexibility for the realization of artificial photonic neurons and brain-inspired photonic computation architectures with a high degree of parallelism. In addition, advances in the field of nanofabrication and photonic integrated circuits (PICs) offer great promise for further reducing the footprint and energy consumption of photonic-based neuromorphic platforms. Over the past decade, a variety of photonic artificial neurons, synapses, and neural networks have been investigated and developed. Various photonic devices have been demonstrated to mimic the dynamic behavior of biological neurons (e.g., spiking), including semiconductor ring lasers [2], quantum dot lasers [3], semiconductor micro-disk lasers [4], optoelectronic oscillators [5], [6], and vertical-cavity surface-emitting lasers (VCSELs) [7]–[9]. Compared to biological neurons, which operate at millisecond timescales, laser-based optical neurons can offer much faster operation speeds in the sub-nanosecond range [10] thanks to their very short carrier lifetimes. Among these approaches, VCSELs have been proven to be feasible photonic devices that can act as excitable optical spiking neurons with significant utility for spike-based neuromorphic computing [11]–[16]. Most of these demonstrations rely on VCSELs exhibiting rich nonlinear dynamics under optical injection. These dynamical properties can be harnessed to elicit controllable optical spikes when subject to the injection of perturbation signals through mechanisms such as polarization switching, phase and amplitude modulated injection locking [17]–[19].

On the other hand, resonant tunneling diodes (RTDs) have also been recently investigated for use as artificial spiking neurons [20]–[22]. The RTD is a unipolar semiconductor device typically consisting of a double-barrier quantum well (DBQW) epilayer heterostructure. The two-dimensional DBQW structure with a thickness of several nanometers introduces the ultrafast resonant quantum tunneling effect [23], [24]. The tunneling current is determined by the quantum tunneling probability, which is substantially controlled by the applied bias voltage. There is a local maximum of the current, resulting in an N-shaped I-V characteristic curve with one or more highly nonlinear negative differential conductance (NDC) region(s) [25], [26]. Thus, RTD-based devices can operate in multiple dynamic regimes depending on the bias voltage. Furthermore, resonant tunneling is a very fast process [27], [28]. When biasing an

RTD in its NDC region, which exhibits an extensive bandwidth, one can observe a self-oscillation with the frequency determined by the RTD and the peripheral circuit elements. Studies of RTD-based oscillators have demonstrated a wide range of oscillation frequencies from tens of GHz [29] to the highest reported 1.98 THz [30]. Because the epitaxial layer structures of RTD are fabricated using common III-V compound semiconductors, such material systems allow the RTD to monolithically integrate with other semiconductor electronic and photonic devices with high degree of integration density. A range of RTD-based electrical/photonic devices has been investigated to emulate the dynamical properties of biological neurons, and some of the dynamical features, such as excitability and refractoriness, have been confirmed in RTD devices, rendering them as a viable solution for controllable spiking generators [22], [31]–[34].

In previous experiments and simulation work, we have investigated some important dynamical behaviors of excitable RTD optoelectronic spiking neurons [22], [35] and the operating mechanisms of RTD-based optical links for signal propagation and information processing tasks [36]. Spike amplitude tuning in synaptic links underpins the weighting functionality, which is key to information processing in spiking neural networks. As a further extension of previous work, the results in this report, for the first time, demonstrate the controllable amplitude tuning of the optical spikes within the RTD-based optoelectronic neuron by simply controlling the bias current of the VCSEL. In particular, we are addressing an RTD-based, VCSEL-coupled artificial optical neuron that allows one to fully tune the presynaptic weighting of their emitted optical spikes at high speed. We employ a micrometer scale InGaAs RTD grown on an InP substrate as the core spiking element in a photodetector-RTD-laser (PRL) layout [22]. First, we experimentally illustrate some basic characteristics of spike firing signals in the proposed RTD-laser optoelectronic spiking neuron. Following that, we demonstrate the functionality of presynaptic optical spike amplitude tuning (weighting) in this optoelectronic neuronal model. By simply tuning the bias current of the laser coupled to the RTD element, we demonstrate precise tuning of the amplitude of the optical spikes, hence enabling an optoelectronic neuron with incorporated spike weighting capability. Importantly, compared to other weight control methods such as external optical modulation using a Mach-Zehnder modulator, direct current control based on the VCSEL gain switching scheme exhibits lower energy consumption and system complexity, thus offering a versatile, effective, yet simple way to achieve presynaptic optical spike weighting. Finally, we further numerically simulate a monolithically integrated nanoscale PRL neuron model to confirm the experimental findings and the ability of the reported optoelectronic spiking neuron to achieve high-speed operation above GHz rates.

2. Methods

The photonic spiking neuron of this work consists of three parts: a photodetector acting as an optical-to-electrical (O-E) receiver; an excitable micrometer-scale RTD producing spikes in response to incoming input perturbations and a (1550 nm) VCSEL acting as an electrical-to-optical (E-O) transmitter. This layout is referred to as the PRL node throughout this work and is depicted in the scheme in Fig. 1(a).

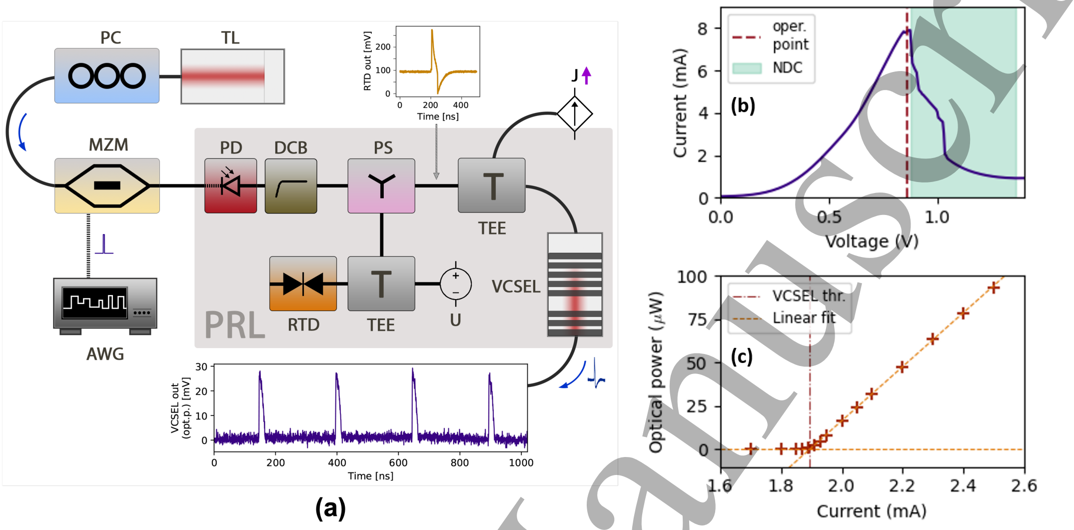

Figure 1. (a) Experimental setup of the PRL spiking neuronal node. The insets present the electrical spikes fired by the RTD upon receiving incoming perturbations and the subsequent optical spikes after E-O conversion by the VCSEL. (b) Measured I-V curve of the RTD. To achieve perturbation-induced spike firing, the operation point is set at a voltage just before the negative differential conductance (NDC) region. (c) Light-current curve of the VCSEL.

The optical input to the PRL is provided by a 1310 nm CW tuneable laser (TL, Santec TSL-210) modulated by a Mach-Zehnder modulator (MZM) with RF signals from an arbitrary waveform generator (AWG, Keysight M8190 12 GSa$\cdot s^{-1}$) via a 10 dB RF amplifier. The modulated light, with encoded optical input perturbations, is received by the O-E module of the PRL neuron, a 9 GHz amplified InGaAs photodetector (PD, Thorlabs PDA8GS). The electrical output from the PD with the encoded input perturbations is subsequently applied to the RTD through a 12 GHz bias tee (Inmet 8800SMF1-12) that simultaneously provides a DC bias voltage for the RTD to function at the desired operating point.

The RTD device (with a 3 µm radius circular mesa) is fabricated by metalorganic vapour-phase epitaxy (MOVPE) on a semi-insulating InP substrate, containing a core 1.7 nm AlAs/5.7 nm InGaAs/1.7 nm AlAs DBQW structure surrounded by highly doped n-InGaAs spacer layers. The RTD under test has ‘signal’ and ‘ground’ bond pads connecting to the collector and emitter electrodes (both n-type) of the RTD epi-layer structure, respectively. The RTD is connected to the voltage source via a ground-signal-ground (GSG) probe landed on the corresponding RTD bond pads. In this work, the forward biasing direction is defined as the RTD collector electrode being linked to the positive pole of the DC source and the I-V characteristic is obtained by sweeping the bias voltage from 0 V up to 1.5 V, as shown in Fig. 1(b). When operating the RTD inside its

NDC region (with a bias above 870 mV), the RTD operates in its self-oscillation mode. To operate the RTD device as an excitable spiking generator, the RTD is DC biased in the positive differential conductance (PDC) region close to the NDC region (≈ 20 mV). In such a setting, the arrival of perturbations with sufficiently strong strength can shift the operating point of the RTD from the PDC region to the NDC region, causing the RTD to fire a spike alongside a fixed limit cycle [32]. Importantly, the I-V curve of RTD devices can be affected by temperature variations, resulting in the shift of the I-V curve and a consequent change in the operating point, which determines the spiking threshold conditions. However, the temperature variation due to the ambient environment and laser illumination in this work is negligible and does not affect the operation of the RTD as the spiking neuron. Therefore, the operation of RTD is implemented at room temperature without designated thermal management. The E/O output of the PRL neuronal node is realized with a standard VCSEL (Raycan) operating at 1550 nm, with a threshold current of 1.95 mA as shown in Fig. 1(c). The VCSEL is driven with an RF-enabled laser mount (Thorlabs LDM56) with thermal control. The electrical spikes generated from the RTD are directly coupled to the laser through a bias tee network. To observe the produced optical spikes at the PRL node's output, the VCSEL signal is passed through an optical isolator and read out on a 16 GHz real-time oscilloscope (RTP, Rohde & Schwarz) using a second amplified photodetector.

3. Results

3.1. Thresholding and refractoriness characterization of the RTD neuron

As the core element of the PRL spiking neuromorphic system, the RTD provides excitability and spiking functionality for the artificial neuron [22]. To trigger the spikes in the PRL, the CW light from the 1310 nm tuneable laser is intensity-modulated via a fiber-coupled MZM (JDS Uniphase). The input perturbations are encoded in the CW light from the TL with a mean power of $\approx 500\,\mu$W. At the input of the PRL, the PD converts this signal to electrical perturbations for the excitable RTD. To illustrate the all-or-nothing thresholding characteristic of the RTD spiking neuron, the modulation signal is configured with a set of square pulses with a pulse length of $t_{len} = 5$ ns and amplitudes gradually increasing from sub-threshold to super-threshold values. Notably, the spiking threshold, which defines the distance from the quiescent state to the spike-firing state, can be adjusted by varying the operating point of the RTD (i.e. the bias voltage of the RTD) [22], therefore the intensity of input stimuli should be modified accordingly. The all-or-nothing thresholding functionality is depicted in Fig. 2(a), where the threshold for spike firing is marked as a dashed line. Since the RTD is biased at an operation point close enough to the NDC region (here $V_{RTD} = 870$ mV), pulses with sufficient (super-threshold) amplitude can elicit spiking responses, while pulses with sub-threshold amplitude do not trigger a spike in the RTD and the system remain quiescent [22].

Additionally, Fig.2(b) depicts another important neuron-like dynamical behavior observed in the PRL. After firing a spike, the PRL neuron exhibits an inactivity time during which it cannot respond to any other incoming stimulus. This is referred to as the refractory (lethargic) period [22]. To investigate this behavior, the input signal is designed with a series of doublets where the interval within each doublet gradually increases from 70 ns to 100 ns, with a 10 ns increment. In the modular PRL system used in this work for proof-of-concept, as indicated in Fig.2(b), the RTD does not fire a second spike for the first two doublets (with t_{sep} =70 ns and 80 ns). However, when the interval within each doublet is above ≈90 ns, the RTD starts to fire the second spike. Thus, the refractory period is estimated to be T_{ref}=90 ns. This defines the maximum repetition rate of spikes at ≈ 10 MHz. In the experimental results (Fig. 3), which demonstrate the tuneability of the presynaptic spike weight in the PRL node, the time interval between consecutive adjacent input perturbations is set equal to 250 ns. This is deliberately above the refractory period of the PRL node to avoid any effects imposed by the refractoriness of the system in its spike weight tuning functionality.

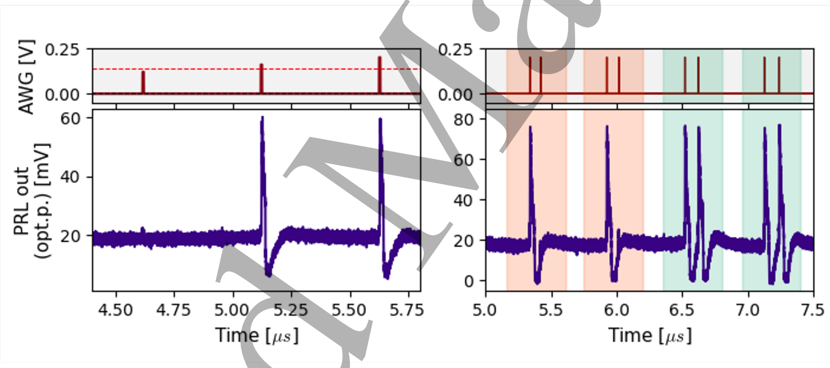

(a) (b)

Figure 2. Spike firing, thresholding and refractoriness characterization of the excitable RTD at the core of the PRL optoelectronic neuronal node. (a) Variations in the amplitude of input perturbations (t_{len} =5 ns optical pulses) result in either a full spike or no response in the system. (b) When the system is fed with doublets (pulse pairs) where the interval within each doublet gradually increases, the RTD can fire the second spike only for those with intervals longer than RTD's refractory period., e.g. the first two doublets t_{sep} =70 ns, 80 ns do not elicit a second spike from the RTD, while doublets with separations of 90 ns, 100 ns do.

3.2. Experimental analysis of optical spike weight tuning in the PRL neuron

Since the laser element (VCSEL) in the PRL node's layout is coupled to the RTD via a bias tee network, the laser driving current can be independently adjusted to perform presynaptic spike amplitude modulation (weighting). The lasing threshold of the VCSEL used here is approximately equal to 1.95 mA. In our experiments, we investigate a range of VCSEL bias currents up to 1.8 mA, which is below its lasing threshold. When the VCSEL operates below its threshold and the RTD remains in the quiescent state, no lasing emission is obtained from the VCSEL. Once the RTD fires an electrical spike following the arrival of an incoming super-threshold optical perturbation ($t_{len} = 2\,\mathrm{ns}$), this electrical spike modulates the VCSEL and shifts its operating point above its lasing threshold momentarily, yielding an optical spike at the PRL's output. Thus, the output optical spikes from the VCSEL preserve most of the features of the incoming electrical spikes. This mechanism can be considered a gain-switched operation, with advantages in a higher signal-to-noise ratio (SNR) of produced spikes and lower power consumption during the non-spiking (quiescent) state. Fig. 3(a-h) shows the measured traces of the PRL output optical spikes for the gradually increased VCSEL bias currents, from 1.1 mA (Fig. 3(a)) to 1.8 mA (Fig. 3(h)) with a step size of 100 µA. These results demonstrate how the amplitude of the optical spikes rises with the increase in the VCSEL bias current, while the signal floor remains at zero (photodetector noise) level as the laser does not lase outside of pulse activation. Longer time traces with spikes are shown for the minimum (1.1 mA, Fig. 3(i)) and maximum (1.8 mA, Fig. 3(j)) investigated current. Finally, Fig. 3(k) reveals a linear relationship between the maximum amplitude of the optical spike and the VCSEL bias current. In particular, unlike in the super-threshold operation mode (as shown in Fig. 2), only the upward part of the spikes is preserved

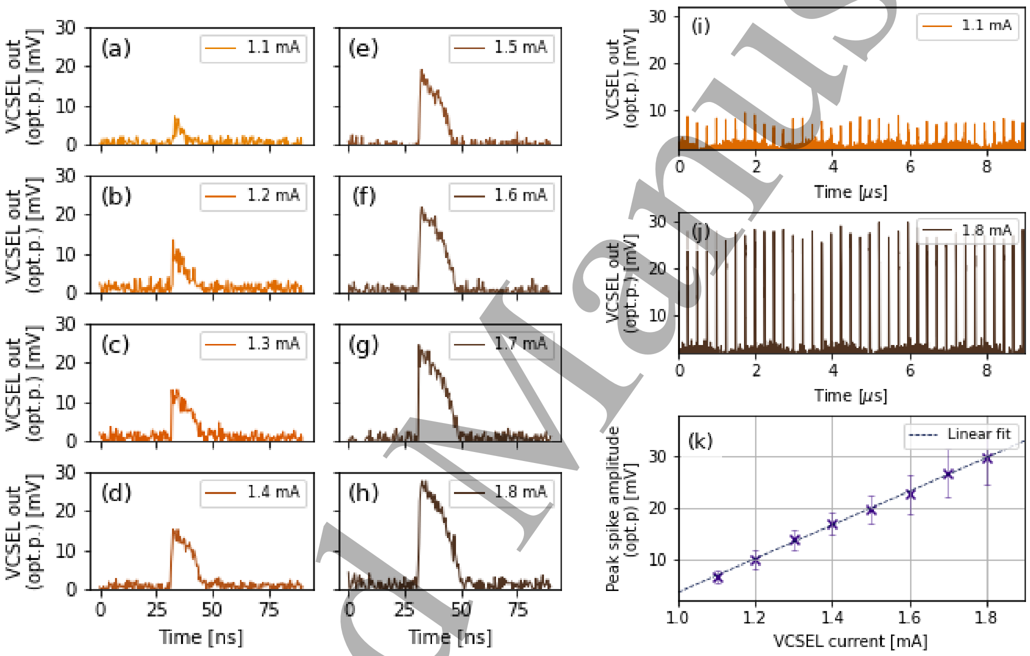

Figure 3. Demonstration of the weighting tuneability of the VCSEL output spike amplitude by tuning the VCSEL bias current. (a)-(h) The amplitude of optical output spikes increases as the bias current is changed from 1.1 mA to 1.8 mA with a step size of 100 µA. All the bias currents are below the lasing threshold. (i) Measured time trace at the VCSEL's output showing the produced optical spikes when the device is biased at 1.1 mA, while (j) shows a trace with spikes for 1.8 mA. (k) Mean amplitudes of the optical spikes as a function of the VCSEL bias current accompanied by a linear fit.

when biasing the VCSEL below or at its threshold due to the gain-switching operation of the VCSEL. This approach offers a viable way to reshape the profile of the output optical spikes which may be beneficial for spike-based signal processing in follow-up downstream nodes.

3.3. Simulation of the ultrafast spike tuneability in the PRL neuron

In this section, a numerical model is implemented in Python and used to validate the optical spike tuneability of the PRL system as demonstrated in the experiment. The PRL model combines an RTD, nanoscale laser and simplified photodetection term coupled via current (with scaling factor κ) to the RTD. The parameters for the I-V characteristic of the RTD [36] and for the laser diode used in this work are representative of nanoscale devices. Although a VCSEL (with a distributed Bragg reflector cavity and multiple-quantum-well active medium) is used in this experiment for the proof-of-concept, this model extrapolates the same functionality towards a nanolaser [37]. Such a model is utilized because future iterations of the PRL will be aimed towards device downscaling and on-chip device integration.

The two-dimensional (current I, voltage V) RTD model coupled with the two-dimensional (photon number S, carrier number N) laser diode model form a system of four ordinary differential equations:

$$C\frac{dV}{dt} = I - f(V) - \kappa S_m(t) \tag{1}$$

$$L\frac{dI}{dt} = V_m(t) - V - RI \tag{2}$$

$$\frac{dS}{dt} = \left(\gamma_m(N - N_0) - \frac{1}{\tau_p}\right) S + \gamma_m N + \sqrt{\gamma_m N S}\,\xi(t) \tag{3}$$

$$\frac{dN}{dt} = \frac{J + \eta I}{q_e} - (\gamma_l + \gamma_m + \gamma_{nr})N - \gamma_m(N - N_0)|E|^2 \tag{4}$$

Additional details on the dynamical model and parameter descriptions are available from previous work [35], [36]. The parameters used for the I-V curve following Schulman's model [38] are $A = -5.5 \times 10^{-5}$, $B = 0.033$, $C = 0.113$, $D = -2.8 \times 10^{-6}$, $N1 = 0.185$, $N2 = 0.045$, $H = 18 \times 10^{-5}$. The circuit parameters used are $R = 5\ \Omega$, $L = 126 \times 10^{-9}$ H, $C = 2 \times 10^{-15}$ F, $\kappa = 3.5 \times 10^{-7}$. The parameters used for the laser model are $N_t = 5 \times 10^5$, $\alpha = 2$, $\tau_p = 5 \times 10^{-13}$ s, $\gamma_m = 1 \times 10^7\ \mathrm{s}^{-1}$, $\gamma_l = 1 \times 10^9\ \mathrm{s}^{-1}$, $\gamma_{nr} = 2 \times 10^9\ \mathrm{s}^{-1}$, $\eta = 0.8$. In contrast to previous work, the J parameter (describing the bias current applied to the laser diode) in this study is not fixed but varied to obtain the desired spike-amplitude tuning effect. The J value is varied between $200\,\mu\mathrm{A}$ and $300\,\mu\mathrm{A}$ with $10\,\mu\mathrm{A}$ increments. The calculated threshold current for the nanoscale laser is $I_{thr} \approx 337\,\mu\mathrm{A}$ [36], meaning all the studied J values are subthreshold. The RTD is biased at $V_0 = 730\,\mathrm{mV}$ (valley point of the NDC region), and this configuration produces positive current spikes that translate into upward pulses (spikes) in the serially coupled laser. A single super-threshold perturbation (100 ps long square shape) is applied to the photodetector term in the nanoscale PRL model, eliciting a single excitable spike that is directly coupled to the nano-laser element via the current term. The results for different J values are shown in Fig. 4(a-j). The simulated I-V curve of the nanoscale RTD is obtained using the provided parameters as shown in Fig. 4(k). The I-V curve also includes a single spiking event shown as a single excursion around the fixed limit cycle in the phase space. It can be clearly observed in Fig.4(a-j) that by varying the term J, a wide range of spike amplitudes can be obtained. As the RTD spikes enter the laser, it briefly shifts the laser operating point above its lasing threshold. Again, operation in the gain-switching regime improves the SNR while keeping the quiescent level below the lasing threshold. The latter is desirable for reducing energy consumption since there is no lasing emission outside of the spiking period. In Fig.4(l), the average spike amplitude (in S) monotonically increases with the rise of the laser driving current and the spike amplitude (calculated with respect to the signal floor) tends to saturate as the laser approaches its lasing threshold current. With a further increase in the bias current, there is no further increase in the spike amplitude in comparison to the baseline optical power. The amplitude saturation effect occurs at $J \approx 270\,\mu\text{A}$ due to the non-zero current contribution from the RTD itself during the steady state. Notably, the experimental results presented in the previous section are used for proof-of-concept demonstration and

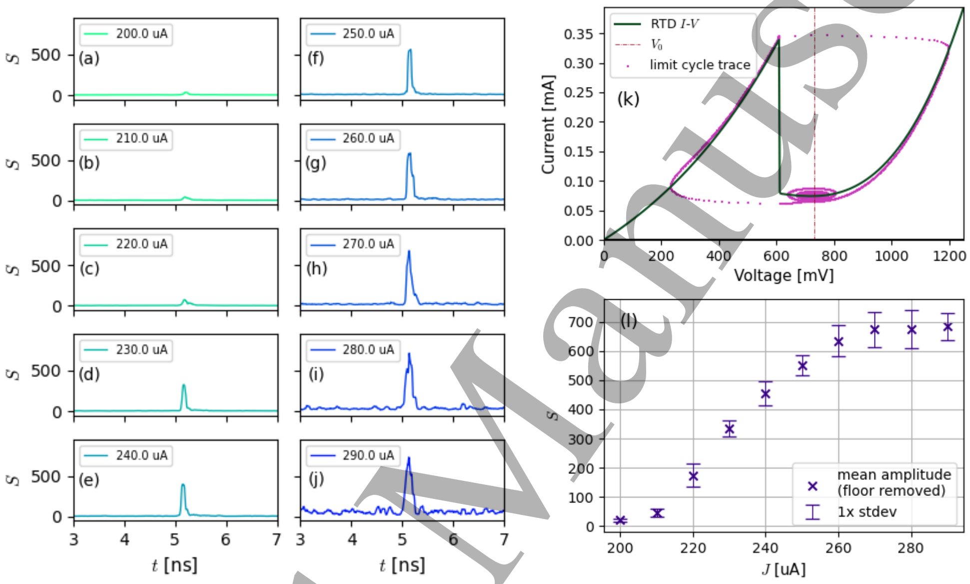

Figure 4. Numerical analysis of the presynaptic spike weighting functionality in the nanoscale PRL neuron, with the RTD biased at its valley point. (a-j) show traces of the optical spikes (in photon count S) corresponding to the gradually incremental laser driving current J. All the time traces are smoothened with 75 ps simple moving average. (k) Simulated I-V curve with a single spike event shown as a trajectory in the phase space. (l) illustrates the spike amplitude (in S) monotonically increases with the rise of the laser driving current. Optical spike amplitude (with respect to the signal floor) reaches saturation as the laser operating point reaches the threshold.

the modular system consists of not only the separative photodetector, RTD and VCSEL, but also other components in the setup (e.g. cables, bias tees, power splitter etc.). These factors may affect the performance of the PRL system (such as spike shapes and firing rates) and result in variation between the experimental and simulation results. Overall, the simulation results are in agreement with the experiments and further validate the viability of the single monolithic integrated optical excitable PRL neuron with current-controlled spike amplitude adjustment functionality operating above GHz rates [35], [36].

4. Conclusions

In summary, we have measured and simulated an optoelectronic spiking neuron based on a RTD coupled to a photodetector and laser (PRL neuron). We show that the PRL delivers deterministic optical spikes, and demonstrate the system's inherent capability of performing presynaptic spike weight tuneability. The experimental demonstration presents a proof-of-concept modular PRL neuronal node built upon a PD, microscale RTD and telecom VCSEL. The RTD fires excitable spikes in response to optical perturbations received on the PD. Subsequently, the spikes fired from the RTD are converted to the optical domain by the VCSEL. The capability of delivering presynaptic spike amplitude tuneability (weighting) along with the neuromorphic excitability in the same node renders the investigated PRL node as highly promising for future optical spiking neural network (SNN) realizations. The functionality of spike weighting is achieved by a simple and highly controllable approach, i.e. by tuning the bias current applied to the laser in the PRL node, therefore avoiding the use of additional optoelectronic weighting elements, such as optical modulators or ring resonators. Moreover, as the bias current of the VCSEL is set below its threshold current, the laser does not emit when the RTD remains in the quiescent state. It allows for spike amplitude adjustment without the presence of persistent lasing emission, which is beneficial for improving the energy efficiency of the idle status and promoting the signal-to-noise ratio of optical spiking. In the simulation, we theoretically validate this functionality using a numerical PRL model describing the operation of a monolithically integrated PRL neuronal node. Our numerical investigation not only confirms the experimental results but also portrays the prospect of low-energy and ultrafast (>GHz rates) nanoscale optoelectronic spiking neurons with inherent optical spiking weighting operation.

For future work, the experimental set-up would be optimized by using high-bandwidth components to achieve a higher spike firing rate. To further reduce footprint and power consumption, the combination of the standalone photodetector and RTD in this prototype PRL layout can be replaced by an optically sensitive RTD (RTD-PD), which directly combines the photodetection and excitable spiking functionality in a single (sub)micrometer-sized device. It allows for the excitability to be triggered by optical perturbations directly without the need for an additional PD element. Therefore, the system-level performance can be improved to allow for higher firing rates accompanied by lower optical/electrical energy and alleviated distortions that occur during signal propagation.

5. Acknowledgements

The authors acknowledge support by the European Commission (Grant 828841-ChipAI-H2020-FETOPEN-2018-2020) and by the UK Research and Innovation (UKRI) Turing AI Acceleration Fellowships Programme (EP/V025198/1). The authors would also like to acknowledge Iwan Davies (IQE plc) for the wafers used to fabricate the RTDs.

References

[1] P. R. Prucnal and B. J. Shastri, *Neuromorphic Photonics*, 1st Editin. Boca Raton: CRC Press, 2017, 440 pp., ISBN: 978-1-4987-2522-4.

[2] W. Coomans, L. Gelens, S. Beri, J. Danckaert, and G. Van der Sande, "Solitary and coupled semiconductor ring lasers as optical spiking neurons," *Physical Review E*, vol. 84, no. 3, p. 036 209, Sep. 19, 2011, Publisher: American Physical Society. DOI: `10.1103/PhysRevE.84.036209`.

[3] J. Robertson, T. Ackemann, L. F. Lester, and A. Hurtado, "Externally-triggered activation and inhibition of optical pulsating regimes in quantum-dot mode-locked lasers," *Scientific Reports*, vol. 8, no. 1, p. 12 515, Dec. 21, 2018, ISSN: 2045-2322. DOI: `10.1038/s41598-018-30758-2`.

[4] T. Van Vaerenbergh, K. Alexander, J. Dambre, and P. Bienstman, "Excitation transfer between optically injected microdisk lasers," *Optics Express*, vol. 21, no. 23, p. 28 922, Nov. 18, 2013, ISSN: 1094-4087. DOI: `10.1364/OE.21.028922`.

[5] B. Romeira, F. Kong, J. M. L. Figueiredo, J. Javaloyes, and J. Yao, "High-speed spiking and bursting oscillations in a long-delayed broadband optoelectronic oscillator," *Journal of Lightwave Technology*, vol. 33, no. 2, pp. 503–510, Jan. 15, 2015, ISSN: 0733-8724, 1558-2213. DOI: `10.1109/JLT.2014.2376775`.

[6] B. Romeira, R. Avó, J. M. L. Figueiredo, S. Barland, and J. Javaloyes, "Regenerative memory in time-delayed neuromorphic photonic resonators," *Scientific Reports*, vol. 6, no. 1, p. 19 510, May 19, 2016, ISSN: 2045-2322. DOI: `10.1038/srep19510`.

[7] Z. Zhang, Z. Wu, D. Lu, G. Xia, and T. Deng, "Controllable spiking dynamics in cascaded VCSEL-SA photonic neurons," *Nonlinear Dynamics*, Nov. 16, 2019, ISSN: 0924-090X. DOI: `10.1007/s11071-019-05339-1`.

[8] M. Hejda, J. Robertson, J. Bueno, and A. Hurtado, "Spike-based information encoding in vertical cavity surface emitting lasers for neuromorphic photonic systems," *Journal of Physics: Photonics*, vol. 2, no. 4, p. 044 001, Aug. 12, 2020, 1 citations (Crossref) [2021-03-05], ISSN: 2515-7647. DOI: `10.1088/2515-7647/aba670`.

[9] J. Robertson, E. Wade, and A. Hurtado, "Electrically controlled neuron-like spiking regimes in vertical-cavity surface-emitting lasers at ultrafast rates," *IEEE Journal of Selected Topics in Quantum Electronics*, vol. 25, no. 6, pp. 1–7, Nov. 2019, ISSN: 1077-260X. DOI: `10.1109/JSTQE.2019.2899040`.

[10] A. Hurtado and J. Javaloyes, "Controllable spiking patterns in long-wavelength vertical cavity surface emitting lasers for neuromorphic photonics systems," *Applied Physics Letters*, vol. 107, no. 24, p. 241 103, Dec. 14, 2015, 59 citations (Crossref) [2022-02-13], ISSN: 0003-6951. DOI: `10.1063/1.4937730`.

[11] J. Robertson, T. Deng, J. Javaloyes, and A. Hurtado, "Controlled inhibition of spiking dynamics in VCSELs for neuromorphic photonics: Theory and experiments," *Optics Letters*, vol. 42, no. 8, p. 1560, 2017, ISSN: 0146-9592. DOI: `10.1364/ol.42.001560`.

[12] A. Skalli, J. Robertson, D. Owen-Newns, *et al.*, "Photonic neuromorphic computing using vertical cavity semiconductor lasers," *Optical Materials Express*, vol. 12, no. 6, p. 2395, Jun. 1, 2022, ISSN: 2159-3930. DOI: `10.1364/OME.450926`.

[13] J. Robertson, J. A. Alanis, M. Hejda, and A. Hurtado, "Photonic synaptic system for MAC operations by interconnected vertical cavity surface emitting lasers," *Optical Materials Express*, vol. 12, no. 4, pp. 1417–1426, Apr. 1, 2022, Publisher: Optica Publishing Group, ISSN: 2159-3930. DOI: `10.1364/OME.450923`.

[14] J. Robertson, P. Kirkland, J. A. Alanis, *et al.*, "Ultrafast neuromorphic photonic image processing with a VCSEL neuron," *Scientific Reports*, vol. 12, no. 1, p. 4874, Dec. 2022, ISSN: 2045-2322. DOI: `10.1038/s41598-022-08703-1`.

[15] J. A. Alanis, J. Robertson, M. Hejda, and A. Hurtado, "Weight adjustable photonic synapse by non-linear gain in a vertical cavity semiconductor optical amplifier," *Applied Physics Letters*, 2021. DOI: `10.1063/5.0064374`.

[16] M. Hejda, J. Robertson, J. Bueno, J. A. Alanis, and A. Hurtado, "Neuromorphic encoding of image pixel data into rate-coded optical spike trains with a photonic VCSEL-neuron," *APL Photonics*, vol. 6, no. 6, p. 060 802, Jun. 1, 2021, ISSN: 2378-0967. DOI: `10.1063/5.0048674`.

[17] Y. Lu, W. Zhang, B. Fu, and Z. He, "Frequency-switched photonic spiking neurons," *Optics Express*, vol. 30, no. 12, p. 21 599, Jun. 6, 2022, ISSN: 1094-4087. DOI: `10.1364/OE.456583`.

[18] R. Al-Seyab, K. Schires, A. Hurtado, I. D. Henning, and M. J. Adams, "Dynamics of VCSELs subject to optical injection of arbitrary polarization," *IEEE Journal of Selected Topics in Quantum Electronics*, vol. 19, no. 4, pp. 1 700 512–1 700 512, Jul. 2013, 24 citations (Crossref) [2022-02-13], ISSN: 1077-260X, 1558-4542. DOI: `10.1109/JSTQE.2013.2239614`.

[19] J. P. Toomey, C. Nichkawde, D. M. Kane, *et al.*, "Stability of the nonlinear dynamics of an optically injected VCSEL," *Optics Express*, vol. 20, no. 9, p. 10 256, Apr. 23, 2012, 17 citations (Crossref) [2022-02-13], ISSN: 1094-4087. DOI: `10.1364/OE.20.010256`.

[20] M. Hänggi and L. O. Chua, "Cellular neural networks based on resonant tunnelling diodes," *International Journal of Circuit Theory and Applications*, vol. 29, no. 5, pp. 487–504, Sep. 2001, ISSN: 00989886. DOI: `10.1002/cta.172`.

[21] B. Romeira, J. M. L. Figueiredo, and J. Javaloyes, "Delay dynamics of neuromorphic optoelectronic nanoscale resonators: Perspectives and applications," *Chaos: An Interdisciplinary Journal of Nonlinear Science*, vol. 27, no. 11, p. 114 323, Nov. 2017, ISSN: 1054-1500. DOI: `10.1063/1.5008888`.

[22] M. Hejda, E. Malysheva, D. Owen-Newns, *et al.*, *Artificial optoelectronic spiking neuron based on a resonant tunnelling diode coupled to a vertical cavity surface emitting laser*, Jun. 22, 2022.

[23] J. Wang, "Monolithic microwave/millimetrewave integrated circuit resonant tunnelling diode dources with around a milliwatt output power," Ph.D. dissertation, University of Glasgow, Glasgow, 2014.

[24] D. Cimbri, J. Wang, A. Al-Khalidi, and E. Wasige, "Resonant tunnelling diodes high-speed terahertz wireless communications - a review," *IEEE Transactions on Terahertz Science and Technology*, pp. 1–1, 2022, ISSN: 2156-342X, 2156-3446. DOI: `10.1109/TTHZ.2022.3142965`.

[25] H. Mizuta, T. Tanoue, and Cambridge University Press, *The physics and applications of resonant tunnelling diodes*. Cambridge: Cambridge University Press, 1995, OCLC: 852653858, ISBN: 978-0-511-62901-3.

[26] B. Ricco and M. Y. Azbel, "Physics of resonant tunneling. the one-dimensional double-barrier case," *Physical Review B*, vol. 29, no. 4, pp. 1970–1981, Feb. 15, 1984, ISSN: 0163-1829. DOI: `10.1103/PhysRevB.29.1970`.

[27] W. R. Frensley, "Quantum transport calculation of the small-signal response of a resonant tunneling diode," *Applied Physics Letters*, vol. 51, no. 6, pp. 448–450, Aug. 10, 1987, ISSN: 0003-6951, 1077-3118. DOI: `10.1063/1.98418`.

[28] T. C. L. G. Sollner, W. D. Goodhue, P. E. Tannenwald, C. D. Parker, and D. D. Peck, "Resonant tunneling through quantum wells at frequencies up to 2.5 THz," *Applied Physics Letters*, vol. 43, no. 6, pp. 588–590, Sep. 15, 1983, ISSN: 0003-6951, 1077-3118. DOI: `10.1063/1.94434`.

[29] W. Zhang, S. Watson, J. Wang, J. Figueiredo, E. Wasige, and A. E. Kelly, "Optical characteristics analysis of resonant tunneling diode photodiode based oscillators," in *2018 IEEE 87th Vehicular Technology Conference (VTC Spring)*, Porto: IEEE, Jun. 2018, pp. 1–6, ISBN: 978-1-5386-6355-4. DOI: `10.1109/VTCSpring.2018.8417889`.

[30] R. Izumi, S. Suzuki, and M. Asada, "1.98 THz resonant-tunneling-diode oscillator with reduced conduction loss by thick antenna electrode," in *2017 42nd International Conference on Infrared, Millimeter, and Terahertz Waves (IRMMW-THz)*, IEEE, Aug. 2017, pp. 1–2, ISBN: 978-1-5090-6050-4. DOI: `10.1109/IRMMW-THz.2017.8066877`.

[31] F. Hartmann, L. Gammaitoni, S. Höfling, A. Forchel, and L. Worschech, "Light-induced stochastic resonance in a nanoscale resonant-tunneling diode," *Applied Physics Letters*, vol. 98, no. 24, pp. 96–99, 2011, ISSN: 00036951. DOI: `10.1063/1.3600329`.

[32] B. Romeira, J. Javaloyes, C. N. Ironside, J. M. L. Figueiredo, S. Balle, and O. Piro, "Excitability and optical pulse generation in semiconductor lasers driven by resonant tunneling diode photodetectors," *Optics Express*, vol. 21, no. 18, p. 20 931, Sep. 9, 2013, ISSN: 1094-4087. DOI: `10.1364/OE.21.020931`.

[33] B. Romeira, J. M. L. Figueiredo, and J. Javaloyes, "NanoLEDs for energy-efficient and gigahertz-speed spike-based sub- neuromorphic nanophotonic computing," *Nanophotonics*, Jun. 25, 2020, ISSN: 2192-8614. DOI: `10.1515/nanoph-2020-0177`.

[34] J. Zhu, T. Zhang, Y. Yang, and R. Huang, "A comprehensive review on emerging artificial neuromorphic devices," *Applied Physics Reviews*, vol. 7, no. 1, p. 011 312, Mar. 2020, ISSN: 1931-9401. DOI: `10.1063/1.5118217`.

[35] M. Hejda, J. A. Alanis, I. Ortega-Piwonka, *et al.*, "Resonant tunneling diode nano-optoelectronic excitable nodes for neuromorphic spike-based information processing," *Physical Review Applied*, vol. 17, no. 2, p. 024 072, Feb. 25, 2022, ISSN: 2331-7019. DOI: `10.1103/PhysRevApplied.17.024072`.

[36] I. Ortega-Piwonka, M. Hejda, J. A. Alanis, *et al.*, "Spike propagation in a nanolaser-based optoelectronic neuron," *Optical Materials Express*, Mar. 18, 2022, ISSN: 2159-3930. DOI: `10.1364/OME.451706`.

[37] B. Romeira and A. Fiore, "Physical limits of NanoLEDs and nanolasers for optical communications," *Proceedings of the IEEE*, vol. 108, no. 5, pp. 735–748, May 2020, ISSN: 0018-9219. DOI: `10.1109/JPROC.2019.2912293`.

[38] J. N. Schulman, H. J. De Los Santos, and D. H. Choi, "Physics-based RTD current-voltage equation," *IEEE Electron Device Letters*, vol. 17, no. 5, pp. 220–222, May 1996, ISSN: 0741-3106, 1558-0563. DOI: `10.1109/55.491835`.